

This work was written as part of one of the author's official duties as an Employee of the United States Government and is therefore a work of the United States Government. In accordance with 17 U.S.C. 105, no copyright protection is available for such works under U.S. Law.

Public Domain Mark 1.0

<https://creativecommons.org/publicdomain/mark/1.0/>

Access to this work was provided by the University of Maryland, Baltimore County (UMBC) ScholarWorks@UMBC digital repository on the Maryland Shared Open Access (MD-SOAR) platform.

Please provide feedback

Please support the ScholarWorks@UMBC repository by emailing scholarworks-group@umbc.edu and telling us what having access to this work means to you and why it's important to you. Thank you.

JGR Space Physics

RESEARCH ARTICLE

10.1029/2022JA031035

Key Points:

- Thermodynamic and momentum budget of tropical migrating semidiurnal tide in the upper mesosphere and lower thermosphere calculated
- Hough modes cannot fully reconstruct tropical migrating semidiurnal tide component of temperature and winds
- Wave–wave interaction and gravity waves significantly affect tropical migrating semidiurnal tide component of temperature and winds

Correspondence to:

C. C. J. H. Salinas,
ccjsalinas@gmail.com





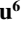

Citation:

Salinas, C. C. J. H., Wu, D. L., Lee, J. N., Chang, L. C., Qian, L., & Liu, H. (2023). Seasonality of the migrating semidiurnal tide in the tropical upper mesosphere and lower thermosphere and its thermodynamic and momentum budget. *Journal of Geophysical Research: Space Physics*, 128, e2022JA031035. <https://doi.org/10.1029/2022JA031035>

Received 21 SEP 2022

Accepted 27 JAN 2023

Seasonality of the Migrating Semidiurnal Tide in the Tropical Upper Mesosphere and Lower Thermosphere and Its Thermodynamic and Momentum Budget

Cornelius Csar Jude H. Salinas^{1,2,3,4} , Dong L. Wu² , Jae N. Lee^{2,5} , Loren C. Chang^{3,4} , Liying Qian⁶ , and Hanli Liu⁶ 

¹Goddard Earth Sciences Technology and Research II, University of Maryland, Baltimore County, Baltimore, MD, USA, ²Earth Sciences Division, NASA Goddard Space Flight Center, Greenbelt, MD, USA, ³Department of Space Science and Engineering, National Central University, Zhongli, Taiwan, ⁴Center for Astronautical Physics and Engineering, National Central University, Zhongli, Taiwan, ⁵Joint Center for Earth Systems Technology, University of Maryland, Baltimore, MD, USA, ⁶High Altitude Observatory, National Center for Atmospheric Research, Boulder, CO, USA

Abstract This work uses the Specified Dynamics-Whole Atmosphere Community Climate Model with Ionosphere/Thermosphere eXtension (SD-WACCM-X) to determine and explain the seasonality of the migrating semidiurnal tide (SW2) components of tropical upper mesosphere and lower thermosphere (UMLT) temperature, zonal wind, and meridional wind. This work also quantifies aliasing due to SW2 in satellite-based tidal estimates. Results show that during equinox seasons, the vertical profiles of tropical UMLT temperature SW2 and zonal-wind SW2's amplitudes have a double-peak structure while they, along with meridional-wind SW2, have a single-peak structure in their amplitudes in June solstice. Hough mode reconstruction reveals that a linear combination of five SW2 Hough modes cannot fully reproduce these features. Tendency analysis reveals that for temperature, the adiabatic term, nonlinear advection term, and linear advection term are important. For the winds, the classical terms, nonlinear advection term, linear advection term, and gravity wave drag are important. Results of our alias analysis then indicate that SW2 can induce an ~60% alias in zonal-mean and DW1 components calculated from sampling like that of the Thermosphere–Ionosphere–Mesosphere Energetics and Dynamics satellite and the Aura satellite. This work concludes that in situ generation by wave–wave interaction and/or by gravity waves plays significant roles in the seasonality of tropical UMLT temperature SW2, zonal-wind SW2, and meridional-wind SW2. The alias analysis further adds that one cannot simply assume that SW2 in the tropical UMLT is negligible.

1. Introduction

The solar migrating semidiurnal tide (SW2) is a westward propagating wavenumber-2 planetary-scale wave with a period of 12 hr. Studies have shown that the solar absorption of stratospheric ozone primarily generates SW2 (Chapman & Lindzen, 1970; Forbes & Garrett, 1979). Its long wavelength allows it to vertically propagate up to the ionosphere/thermosphere (I/T) region (Chapman & Lindzen, 1970). While it propagates, it has been shown to interact with the background atmosphere and/or atmospheric waves such as planetary-scale waves and gravity waves (Angelats i Coll & Forbes, 2002; Forbes, 1982; Forbes & Wu, 2006; Forbes et al., 1995, 2008; Lindzen & Hong, 1974; Palo et al., 1999; Pedatella & Forbes, 2010; Teitelbaum & Vial, 1991; Teitelbaum et al., 1989; van Caspel et al., 2022; Walterscheid & Venkateswaran, 1979a, 1979b; Yamashita et al., 2002; J. Zhang et al., 2021).

SW2 in the tropical upper mesosphere and lower thermosphere (UMLT) region (between 85 and 100 km) is largely ignored because most studies focus on SW2's variability in the middle- to high-latitude UMLT where its amplitudes are known to be the largest (A. H. Manson et al., 2002; Q. Wu et al., 2011). These studies often analyze the interactions of SW2 with winter-prominent phenomena like sudden stratospheric warmings and stationary planetary-scale waves (Angelats i Coll & Forbes, 2002; Forbes & Wu, 2006; Forbes et al., 2008; Limpasuvan et al., 2016; Palo et al., 1999; Pedatella & Forbes, 2010; Teitelbaum & Vial, 1991; Teitelbaum et al., 1989; van Caspel et al., 2022; Yamashita et al., 2002; J. Zhang et al., 2021).

The motivation of this work is studies showing that the 12-hr component of horizontal winds in the tropics observed by ground-based instruments exhibit noteworthy amplitudes and variabilities that 3D models cannot reproduce. Numerous ground-based instruments have observed that the 12-hr oscillation component of tropical

UMLT horizontal winds exhibits significant altitudinal variations. Observations also show that localized peak amplitudes of these 12-hr oscillation are comparable to the amplitudes of the often more dominant 24-hr oscillations (Deepa et al., 2006; A. Manson et al., 1999; Reddi & Ramkumar, 1997; Vincent et al., 1998). Reddi and Ramkumar (1997) and Deepa et al. (2006) reported that meteor wind radar observations of 12-hr oscillations in zonal and meridional winds at Trivandrum (latitude 8°N) from 1984 to 1988 had, for all seasons, significant altitudinal variations present in the 12-hr oscillation amplitude vertical profiles. They then compared them with 24-hr oscillation amplitudes and found that the 12-hr amplitudes exhibited local peaks with magnitudes comparable to the 24-hr oscillations. Vincent et al. (1998) and A. Manson et al. (1999) reported medium frequency radar observations of 12-hr oscillations in horizontal winds at Christmas Island (latitude 2°N) and Hawaii (latitude 22°N) and found 12-hr oscillation amplitudes having features similar to that at Trivandrum. These studies also presented the phases of these 12-hr oscillations. These phases indicated that wavelengths were consistently greater than 100 km (Deepa et al., 2006; A. Manson et al., 1999; Reddi & Ramkumar, 1997; Vincent et al., 1998).

Studies that compared these ground-based observations with linear models showed that the linear models such as the Forbes and Vial (1989) tidal model and the Global Scale Wave Model (GSWM) could not reproduce the significant altitudinal variation in 12-hr oscillation amplitudes. These models consistently simulated 12-hr oscillation amplitude profiles exhibiting only an exponential increase with height (Deepa et al., 2006; A. Manson et al., 1999; Reddi & Ramkumar, 1997; Vincent et al., 1998). Local maximum peaks were not found between 80 and 100 km and their simulated phases also differed from observations. Their simulated phases indicated shorter vertical wavelengths. On the other hand, 3D (3D) first-principles atmospheric general circulation models simulated 12-hr oscillations whose amplitudes exhibited local peaks between 85 and 100 km (Davis et al., 2013; Du et al., 2007) compared horizontal wind observations at Ascension Island (latitude 8°S) from 2002 to 2011 with simulations from 3D whole atmosphere models called the Canadian Middle Atmosphere Model (CMAM) and the Specified Dynamics-Whole Atmosphere Community Climate Model (SD-WACCM). Their results show the simulations exhibiting significantly more altitudinal variation in the 12-hr oscillations amplitude although the variation is not the same as observed. Their results also showed that WACCM 12-hr oscillation phases were indicative of the (2,2) mode. However, their work does not determine the contributions of SW2 in these 12-hr oscillations. On the other hand, Du et al. (2007) analyzed 12-hr oscillations from meteor radar observations in Jakarta (latitude 6°S) and Kotobabang (latitude 0°) and compared them with CMAM simulations. They found that the SW2 component does contribute the most to the 12-hr oscillations in these regions. The ability of 3D models to, at the very least, capture the significant altitude variation of SW2's amplitude over the tropics indicates that nonclassical and nonlinear processes may primarily drive SW2 in the tropics. To our knowledge, no study has analyzed this in-depth.

Space-based instruments that can resolve the SW2 component of horizontal winds in the tropical UMLT include the High Resolution Doppler Imager onboard the Upper Atmosphere Research Satellite as well as the Thermosphere-Ionosphere-Mesosphere Energetics and Dynamics (TIMED) Doppler Interferometer instrument onboard the TIMED satellite (Burrage, Hagan, et al., 1995; Burrage, Wu, et al., 1995; Forbes & Wu, 2006; Forbes et al., 2008; McLandress et al., 1996; Oberheide et al., 2007; Pancheva et al., 2009; Q. Wu et al., 2003, 2006; Yuan et al., 2008; X. Zhang et al., 2006). Unfortunately, nobody has done any in-depth analysis of the SW2 component of horizontal winds solely in the tropical UMLT region with these instruments because, as mentioned earlier, focus has always been on the regions where amplitudes are the highest which are over the middle to high latitudes.

Doing an in-depth analysis of SW2 in the tropical UMLT region is important in fully understanding the dynamics in the region. This is crucial to accurate space weather forecasting. Wave-wave interaction in the region continues to be difficult to understand and to forecast. Numerous studies have already shown that traveling planetary waves from other latitudes interact with the migrating diurnal tide which is the most dominant migrating tide in the UMLT region (Chang et al., 2011; Forbes & Zhang, 2017). On the other hand, minimal work presents an understanding on how these waves interact with SW2 because its amplitude is weak in this region. However, based on the studies using ground-based instruments, linear models, and 3D models, there are altitudes in the tropical UMLT where SW2's amplitudes may be significant enough that it could be involved in wave-wave interactions with other planetary waves. In the middle to high latitudes, SW2 has been shown to interact with these planetary-scale waves and form nonmigrating tides (Angelats i Coll & Forbes, 2002; Forbes & Wu, 2006; Forbes et al., 2008; Limpasuvan et al., 2016; Palo et al., 1999; Pedatella & Forbes, 2010; Teitelbaum & Vial, 1991; Teitelbaum et al., 1989; van Caspel et al., 2022; Yamashita et al., 2002; J. Zhang et al., 2021). Thus,

understanding this complexity in SW2's amplitudes over the tropical UMLT is important in knowing more of these other wave-wave interactions.

Doing an in-depth analysis of SW2 in the tropical UMLT region is also important in analyzing satellite measurements with limited local-time coverages. Two-dimensional least squares fit is one of the more reliable ways to estimate both the daily-mean zonal-mean component and atmospheric wave components of a given atmospheric parameter if the data achieve full local-time coverage (D. L. Wu et al., 1995). This method mitigates aliasing. However, for the analysis of short-term variabilities, other methods are currently being utilized that tend to make assumptions on the presence of particular atmospheric waves (Oberheide et al., 2003). One well-known approach is applied on observations from sun-synchronous satellites. These sun-synchronous satellites typically only provide global observations at two local times. Over the equator, these local times are around 12 hr apart. To get the daily-mean zonal-mean profile for a day, studies commonly just average these values with the assumption that SW2 is negligible. This is done with the assumption that SW2 amplitudes are negligible, and this assumption is believed to always be true over the equator even though minimal work has been done to investigate SW2 in the region.

This work aims to further our understanding of SW2 by investigating the seasonality of SW2 in the tropical UMLT using the Specified Dynamics-Whole Atmosphere Community Climate Model with Ionosphere/Thermosphere eXtension (SD-WACCM-X). Using a multiyear run of SD-WACCM-X that spans from 2000 to 2019, this work determines the seasonal climatology of the SW2 component of UMLT temperature and horizontal winds averaged over the tropics. Then, this work quantifies the contributions of Hough modes to these features as well as determining the thermodynamic and momentum budget behind these features. Finally, we quantify the tidal aliases involving SW2 when one uses satellite-based instruments. Since observational studies have ignored SW2 over the tropics, nobody has done any thorough analysis of tidal aliases involving SW2. We are specifically going to determine the alias due to the most dominant tide in this region, the migrating diurnal tide (DW1). By doing all these analyses, this work not only aims to further our understanding of SW2 in the tropical UMLT region, but this work also aims to be a springboard for in-depth analysis of SW2 in this region using satellite-based observations.

2. Methodology

There are two parts in our analysis. The first part presents and explains the seasonality of SD-WACCM-X SW2 in tropical UMLT temperature, zonal wind, and meridional wind. The second part is an alias test to quantify the aliasing involving SW2. In this section, we first present the model and the diagnostics involved in presenting and explaining the seasonality of SD-WACCM-X SW2. The second part presents the observations used to create an artificial data set that will be used for the alias analysis.

2.1. SD-WACCM-X Simulations and Diagnostics

2.1.1. SD-WACCM-X Model

WACCM-X is a first-principles physics-based model that simulates the whole atmosphere from the surface to the ionosphere/thermosphere while accounting for the coupling of the atmosphere with the ocean, sea ice, and land. Davis et al. (2013) showed that the WACCM can simulate SW2 amplitudes in the tropical E-region that exhibited local maxima. WACCM simulates the atmosphere from the surface of the Earth to around 140 km. WACCM's tropical E-region, which is between 90 and 110 km, contains minimal ionosphere electrodynamics. On the other hand, WACCM-X simulates the atmosphere from the surface of the Earth to around 700 km and it incorporates a more accurate ionosphere. For more descriptions on the model, see H. L. Liu et al. (2018) and J. Liu et al. (2018). WACCM-X is a model that combines WACCM with elements of the thermosphere ionosphere general circulation models. SD-WACCM-X is a version of the WACCM-X that is nudged by the Modern-Era Retrospective Analysis for Research and Applications reanalysis data set from the surface to around 50 km (Marsh et al., 2013; Rienecker et al., 2011). This ensures that the atmosphere from the surface of the Earth to the stratosphere is realistic in all simulations. We build off Davis et al. (2013) by utilizing a model with a more accurate ionosphere as well as by doing a more in-depth analysis of SW2's seasonality in the tropical E-region.

We ran the model from 2000 to 2019 with a horizontal resolution of 1.9° in latitude and 2.5° in longitude and a vertical resolution of two points per scale height below ~ 50 km and four points per scale height above ~ 50 km.

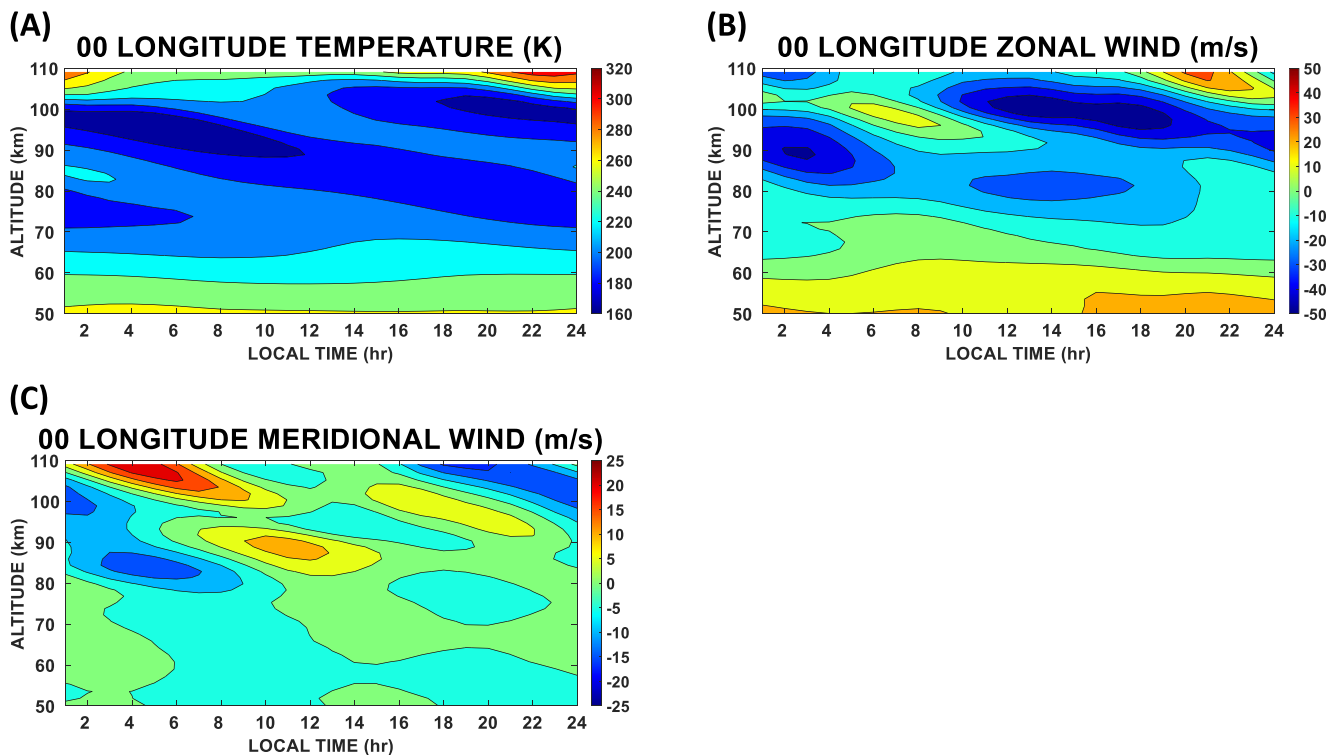


Figure 1. March Equinox SD-WACCM-X temperature (a), zonal wind (b) and meridional wind (c) averaged between latitudes 10°S and 10°N and at longitude 0° as a function of altitude and local time.

We then calculated the monthly means of all the output variables from these simulations. From these monthly means, we calculated the seasonal climatology of each parameter. For example, when this paper mentions temperature in March, this refers to averages of temperature for all March months between 2002 and 2019. We then performed our analysis and model diagnostics on these monthly mean parameters.

Atmospheric tides are global phenomena. Hence, to fully resolve them, one needs a data set that attains global and full local-time coverage in a day (Oberheide et al., 2003). Unfortunately, no such observational data set exists. Ground-based instruments can give you full local-time coverage in a day but not global coverage. Figure 1 shows the altitude–local-time profiles of March temperature, zonal wind, and meridional wind averaged between latitudes 10°S and 10°N over 0° longitude as simulated by SD-WACCM-X. This is what a ground-based instrument over the tropics and at 0° longitude would observe. Figure 1a shows that for this sample case, temperature appears to be dominated by a 24-hr oscillation/diurnal tide. On the other hand, Figure 1b shows how a 12-hr oscillation/semidiurnal tide could manifest alongside a diurnal tide. Between 90 and 100 km, this zonal-wind profile shows westerly winds over 4 a.m. to 12 noon local time and by easterly winds the rest of the day. If the diurnal tide dominated this region, periods of westerly winds and easterly winds should each last exactly 12 hr. Yet, here we see easterly winds dominating most of the day. This indicates that both diurnal and semidiurnal tides are strong. Figure 1c shows how an atmospheric parameter varies if the semidiurnal tide is most dominant. Between 80 and 100 km, we can see southward winds occurring between midnight and 8 a.m. local time as well as between noon and 6 p.m. local time. Northward winds occur over the other local times. While one can clearly determine the periodicities of the dominant tides from this perspective, one cannot determine the wavenumber of the tides.

Satellite-based observations can give you global coverage in a day but not full local-time coverage. One needs to utilize multiple months of data to attain full local-time coverage. Even then, one still must assume that tidal variabilities at daily timescales are not important. Currently, only 3D first-principles physics-based models can give us both global coverage and full local-time coverage in a day. Until we develop the most ideal observational data set, these models offer a satisfactory option to furthering our understanding of these tides.

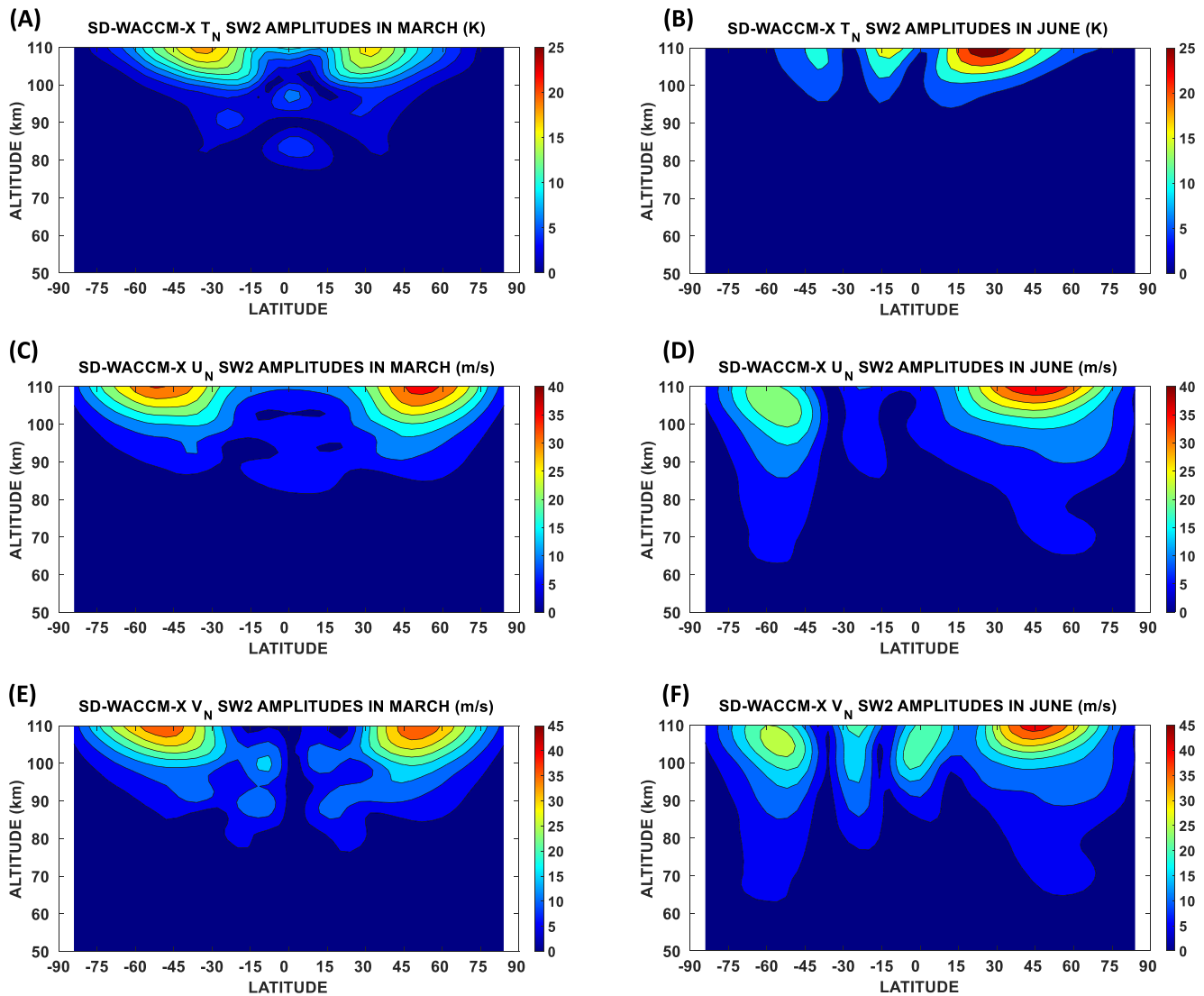


Figure 2. Migrating semidiurnal tide amplitudes of (a) temperature in March equinox, (b) temperature in June solstice, (c) zonal wind in March equinox, (d) zonal wind in June solstice, (e) meridional wind in March equinox, and (f) meridional wind in June solstice.

2.1.2. Two-Dimensional Least Squares Fit

To calculate the SW2 amplitudes and phases of a particular parameter, this work uses two-dimensional least squares fit. The fit uses basis functions of the following form (D. L. Wu et al., 1995):

$$X(\lambda, t) = \bar{X} + \sum_{n=1}^3 \sum_{s=-4}^4 \hat{X}_{n,s} \cos(n\Omega t - s\lambda - \hat{\psi}_{n,s}) + \sum_{s=1}^4 \hat{X}_s \cos(s\lambda - \hat{\psi}_s) \quad (1)$$

Here, X is any atmospheric parameter. \bar{X} is the daily-mean zonal-mean component of the parameter. The second summation term comprises of the migrating and nonmigrating diurnal ($n = 1$), semidiurnal ($n = 2$), and terdiurnal ($n = 3$) tide components with wavenumbers (s) from -4 to 4 . The third summation term comprises of the stationary planetary waves with wavenumbers from 1 to 4 . \hat{X} and $\hat{\psi}$ are the amplitudes and phases, respectively.

Figure 2 shows sample calculations of SW2 amplitudes for temperature, zonal wind, and meridional wind for both an equinox month and a solstice month in the UMLT. Figure 2a shows the SW2 amplitudes for temperature in March equinox peaking to around 20 K above 100 km over the northern and southern midlatitudes. Figure 2b shows the SW2 amplitudes for temperature in June solstice peaking over the northern midlatitudes with values

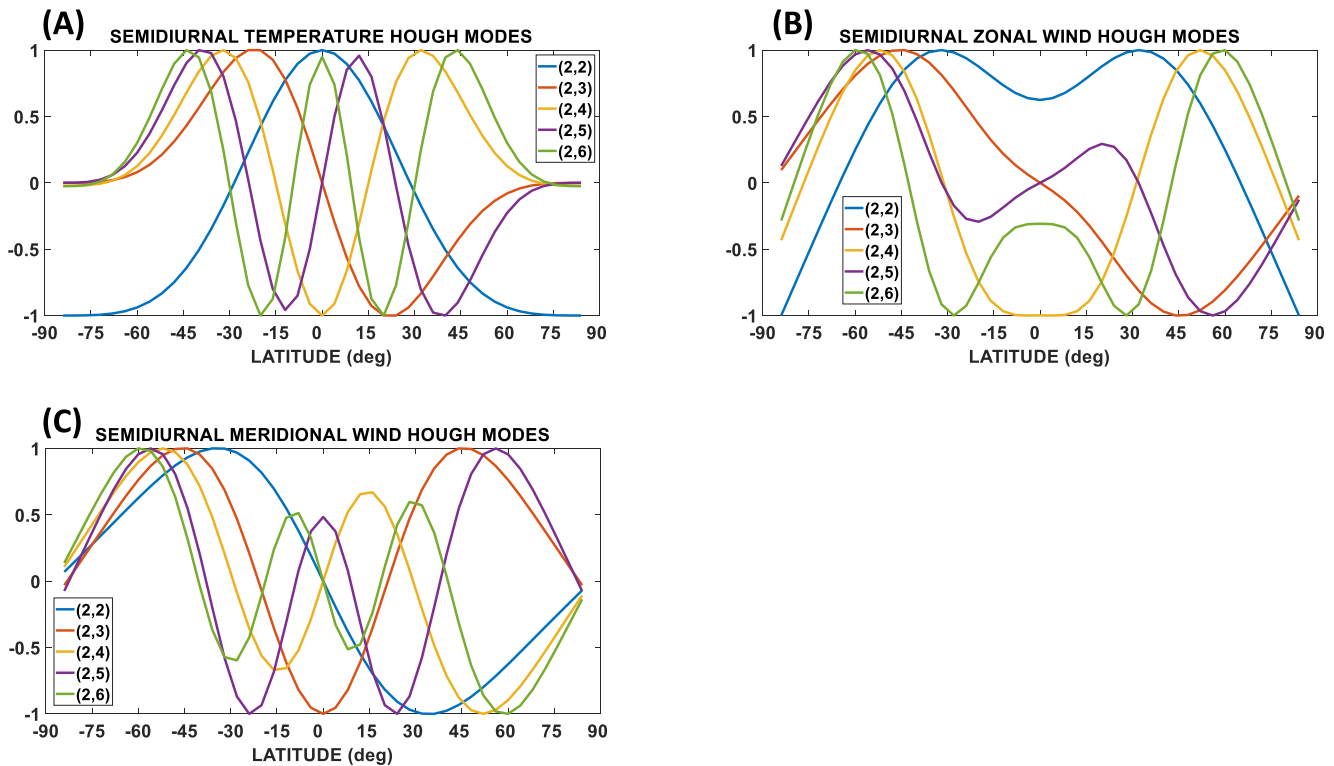


Figure 3. Semidiurnal temperature (a), zonal wind (b), and meridional wind (c) Hough modes. In these plots, the modes are normalized to have values solely between -1 and 1 but for the Hough mode reconstruction calculations, the modes are not normalized.

reaching around 25 K. Figure 2c shows the SW2 amplitudes for zonal wind in March equinox peaking over the northern and southern high latitudes with values reaching around 35 m/s. Figure 2d shows the SW2 amplitudes for zonal wind in June solstice peaking over the northern midlatitudes with values reaching around 35 m/s. Figure 2e shows the SW2 amplitudes for meridional wind in March equinox. It peaks over regions like where zonal-wind SW2 peaks in March equinox. Figure 2f shows the SW2 amplitudes for meridional wind in June solstice and it also peaks over regions like where zonal-wind SW2 peaks in June solstice. As mentioned above, previous studies have already extensively explored these regions of maximum amplitudes (A. H. Manson et al., 2002; Q. Wu et al., 2011). This paper focuses on exploring the amplitudes over the low latitudes. Figure 2a shows a preview of this paper's focus. Figure 2a shows local maximum in temperature SW2 amplitudes over the low latitudes.

2.1.3. Hough Mode Reconstruction

To explain the seasonality of the SW2 components of tropical MLT temperature, zonal wind, and meridional wind, we perform two model diagnostics. The first diagnostic is a Hough mode reconstruction of these components. This involves reconstructing these SW2 components in terms of the five SW2 Hough modes shown in Figure 3. These five SW2 Hough modes have been identified to explain significant variability of SW2 in the high latitudes (Pedatella et al., 2021). This analysis will determine if the same Hough modes can explain SW2 in the tropics. Note that each dynamical parameter has its own set of Hough modes. Figure 3a shows the Hough modes for temperature. Figure 3b shows the Hough modes for zonal wind. Figure 3c shows the Hough modes for meridional wind. Classical linear tidal theory shows that a tide manifests as Hough modes. Hough modes are eigen-solutions to the linearized primitive equations in spherical coordinates assuming the background atmosphere is isothermal, and the zonal mean winds are zero. When tide-mean wind interactions are accounted for, linear tidal theory shows that the mode distortion can be reproduced by superimposing Hough modes according to the relative amplitudes demanded by orthogonal decomposition (Lindzen & Hong, 1974). Hence, this analysis determines if the background atmosphere's distortion of these modes as they vertically propagate primarily drive the seasonality of the SW2 components of tropical MLT temperature, zonal wind, and meridional wind.

This process begins by decomposing the SW2 components of temperature, zonal wind, and meridional wind into Hough modes. To present this process, we use the SW2 component of temperature as an example. We first take

the latitude profile of tropical MLT region temperatures' SW2 amplitudes and phases $\bar{A}(\phi)$ and $\theta(\phi)$ at each altitude z (ϕ is latitude) and construct a new latitude profile whose elements are a complex number $M(\phi) = Ai + B$ where $A = \bar{A}\cos\left(\frac{2\pi\theta}{12}\right)$ and $B = \bar{A}\sin\left(\frac{2\pi\theta}{12}\right)$. This is the complex number formulation of the same tide. Then, we regress $M(\phi)$ with a Hough function indexed j . This gives complex regression coefficients $\sigma_j(z)$ for each Hough mode. This complex number is then used to calculate the amplitude and phase of each Hough mode component.

We then use these complex regression coefficients to construct a new latitude profile $M'(\phi)$ at each altitude z as $M'(\phi) = A'(\phi)i + B'(\phi) = \sum_{j=1}^5 \sigma_j \Theta_j(\phi)$ where $\Theta(\phi)$ corresponds to a Hough function and ϕ corresponds to latitude. This new latitude profile will have elements that are complex numbers. Finally, for each element in the profile, we take the complex number and calculate amplitudes and phases as $\bar{A}'(\phi) = \sqrt{A'^2(\phi) + B'^2(\phi)}$ and $\theta'(\phi) = \tan^{-1}\left[\frac{B'(\phi)}{A'(\phi)}\right]$. $\bar{A}'(\phi)$ and $\theta'(\phi)$ are the amplitudes and phases of the reconstructed SW2 component. The same process is applied to zonal-wind and meridional wind's SW2 components.

2.1.4. Tendency Analysis of the Thermodynamic and Momentum Equation

The second diagnostic is a tendency analysis of the thermodynamic and momentum equations. The thermodynamic equation used in this tendency analysis is given by

$$\frac{\partial T}{\partial t} = -\vec{V} \cdot \nabla T + \frac{\omega RT}{c_p P} + Q_{\text{diab}} \quad (2)$$

In this equation, T is temperature, t is time in seconds, and ω is vertical velocity in Pa/s. P is atmospheric pressure in Pa, R is the gas constant for dry air which is equivalent to 287.058 J/kg/K, and c_p is specific heat of dry air at constant pressure which is equivalent to 1005 J/kg/K. The left-hand side of Equation 2 is the time-derivative of temperature. The right-hand-side terms are the total advection term, adiabatic heating/cooling term, and diabatic heating term. The diabatic heating term is the sum of chemical heating, Joule heating, long-wave heating, nonlocal thermodynamic equilibrium long-wave heating, short-wave heating, CO₂ near-infrared (IR) heating, CO₂ IR cooling, NO IR cooling, extreme ultraviolet (EUV) heating, non-EUV photolysis heating, and heating due to parameterized gravity waves. The goal of this tendency analysis is to determine what terms on the right-hand-side contributes the most to the SW2 amplitude of the time-derivative of temperature. This analysis begins by calculating all the terms in this equation and then calculating their SW2 amplitudes. The total advection term in this equation is calculated as

$$F_{\text{adv},T} = -\vec{V} \cdot \nabla T = -\left(\frac{u}{a \cos \phi} \frac{\partial T}{\partial \lambda} + \frac{v}{a} \frac{\partial T}{\partial \phi} + w \frac{\partial T}{\partial z}\right) \quad (3)$$

In this equation, u is zonal wind, v is meridional wind, w is vertical wind all in m/s, and ϕ is latitude. λ is longitude, z is log-pressure height, and a is the radius of Earth which is equal to 6.36×10^6 m. The terms in the right-hand side are advection of temperature due to zonal wind, meridional wind, and vertical wind.

Advection is further split into linear and nonlinear advection. To do this, we substitute $u = \bar{u} + u'$, $v = \bar{v} + v'$, $w = \bar{w} + w'$, and $T = \bar{T} + T'$ into Equation 3. Terms with overbars denote daily-mean zonal mean and primed terms are perturbations from the daily-mean zonal mean. From the resulting equation, the linear advection term is this section of the equation:

$$F_{\text{linAdv},T} = \frac{\bar{u}}{a \cos \theta} \frac{\partial T'}{\partial \lambda} + \frac{\bar{v}}{a} \frac{\partial T'}{\partial \theta} + \frac{v'}{a} \frac{\partial \bar{T}}{\partial \theta} + \frac{\bar{w}}{a} \frac{\partial T'}{\partial z} + w' \frac{\partial \bar{T}}{\partial z} \quad (4)$$

This equation shows that linear advection includes the advection of mean winds by temperature perturbations as well as the advection of temperature perturbations by the mean winds. Calculation of nonlinear advection explicitly is difficult because it involves atmospheric wave decomposition. To determine the relative importance of nonlinear advection, we opt to just compare the SW2 component of total advection and linear advection. Gu and Du (2018) employed a similar analysis to determine the thermodynamic budget behind the migrating diurnal tide.

The momentum equations used in this tendency analysis are given by

$$\frac{\partial u}{\partial t} = f v - \frac{1}{a \cos \lambda} \frac{\partial \Phi}{\partial \lambda} - \vec{V} \cdot \nabla u + \frac{uv}{a} \tan \phi + F_{GW,x} \quad (5)$$

$$\frac{\partial v}{\partial t} = -f u - \frac{1}{a} \frac{\partial \Phi}{\partial \phi} - \vec{V} \cdot \nabla v + \frac{u^2}{a} \tan \phi + F_{GW,y} \quad (6)$$

In these equations, f is the Coriolis parameter, Φ is geopotential height, and $F_{GW,x}$ and $F_{GW,y}$ are the gravity wave zonal and meridional drag. Equation 5 is the momentum equation for zonal wind, while Equation 6 is the momentum equation for meridional wind. For both cases, the terms on the right-hand side are the Coriolis force, pressure gradient force, advection, curvature, and gravity wave drag. Like the thermodynamic equation, our tendency analysis of the momentum equations determines what terms on the right-hand-side contributes the most to the SW2 amplitude of the time-derivative of zonal wind and meridional wind. Thus, this will also involve calculating each term in this equation and then calculating their SW2 amplitudes. The total advection terms are expressed as follows:

$$F_{adv,x} = -\vec{V} \cdot \nabla u = -\left(\frac{u}{a \cos \phi} \frac{\partial u}{\partial \lambda} + \frac{v}{a} \frac{\partial u}{\partial \phi} + w \frac{\partial u}{\partial z} \right) \quad (7)$$

$$F_{adv,y} = -\vec{V} \cdot \nabla v = -\left(\frac{u}{a \cos \phi} \frac{\partial v}{\partial \lambda} + \frac{v}{a} \frac{\partial v}{\partial \phi} + w \frac{\partial v}{\partial z} \right) \quad (8)$$

The linear advection term is expressed as follows:

$$F_{linAdv,x} = -\vec{V} \cdot \nabla u = -\left(\frac{\bar{u}}{a \cos \phi} \frac{\partial u'}{\partial \lambda} + \frac{\bar{v}}{a} \frac{\partial u'}{\partial \phi} + \frac{v'}{a} \frac{\partial \bar{u}}{\partial \phi} + \bar{w} \frac{\partial u'}{\partial z} + w' \frac{\partial \bar{u}}{\partial z} \right) \quad (9)$$

$$F_{linAdv,y} = -\vec{V} \cdot \nabla v = -\left(\frac{\bar{u}}{a \cos \phi} \frac{\partial v'}{\partial \lambda} + \frac{\bar{v}}{a} \frac{\partial v'}{\partial \phi} + \frac{v'}{a} \frac{\partial \bar{v}}{\partial \phi} + \bar{w} \frac{\partial v'}{\partial z} + w' \frac{\partial \bar{v}}{\partial z} \right) \quad (10)$$

Like the tendency analysis with the thermodynamic equation, to determine the relative importance of nonlinear advection in these horizontal winds, we opt to just compare the SW2 components of their total advection and linear advection terms. Lu et al. (2012) employed a similar analysis to determine the momentum budget behind the migrating diurnal tide.

The results of these tendency analyses will complement the results of the Hough mode analysis. The argument that Hough modes can be used to mathematically express global tidal modes assumes that the tides in our atmosphere behave according to classical tidal theory. In classical tidal theory, it is assumed that temperature is only controlled by adiabatic heating/cooling while winds are only controlled by the Coriolis force and the pressure gradient force. Our Hough mode analysis only determines if the seasonality of tropical MLT temperature, zonal-wind, and meridional wind's SW2 components can be explained by classical tidal theory. Our tendency analysis will determine the specific classical or nonclassical physical processes driving it.

2.2. Satellite Observations and Alias Test

2.2.1. Satellite Observations

For our alias test, this work utilizes the longitude and UT information of temperature observations from the Sounding of the Atmosphere using Broadband Emission Radiometry (SABER) instrument onboard the TIMED satellite as well as the Microwave Limb Sounder (MLS) onboard the NASA Aqua satellite. SABER has alternating latitudinal coverage of 82°N–53°S and 53°N–82°S that occurs due to the TIMED spacecraft yaw cycle every ~60 days (Russell et al., 1999). The mission has an orbital period of ~1.6 hr and a local-time precession of 12 min per day. This orbit allows SABER to achieve full diurnal coverage after 60 days (X. Zhang et al., 2006). This work uses SABER temperature longitude and UT information from profiles between day 60 and day 120 of year 2005. On the other hand, the Aura satellite is in a sun-synchronous orbit. The ascending nodes of the Aura orbit, when the spacecraft is moving toward the north, cross the equator at 1:45 ± 15 p.m. (short-handed to 2 p.m. hereafter) local time. Similarly, the descending nodes, when the spacecraft is moving toward the south, cross the equator at 1:45 ± 15 a.m. (short-handed to 2 a.m. hereafter) local time (<https://aura.gsfc.nasa.gov/scinst.html>). This orbit

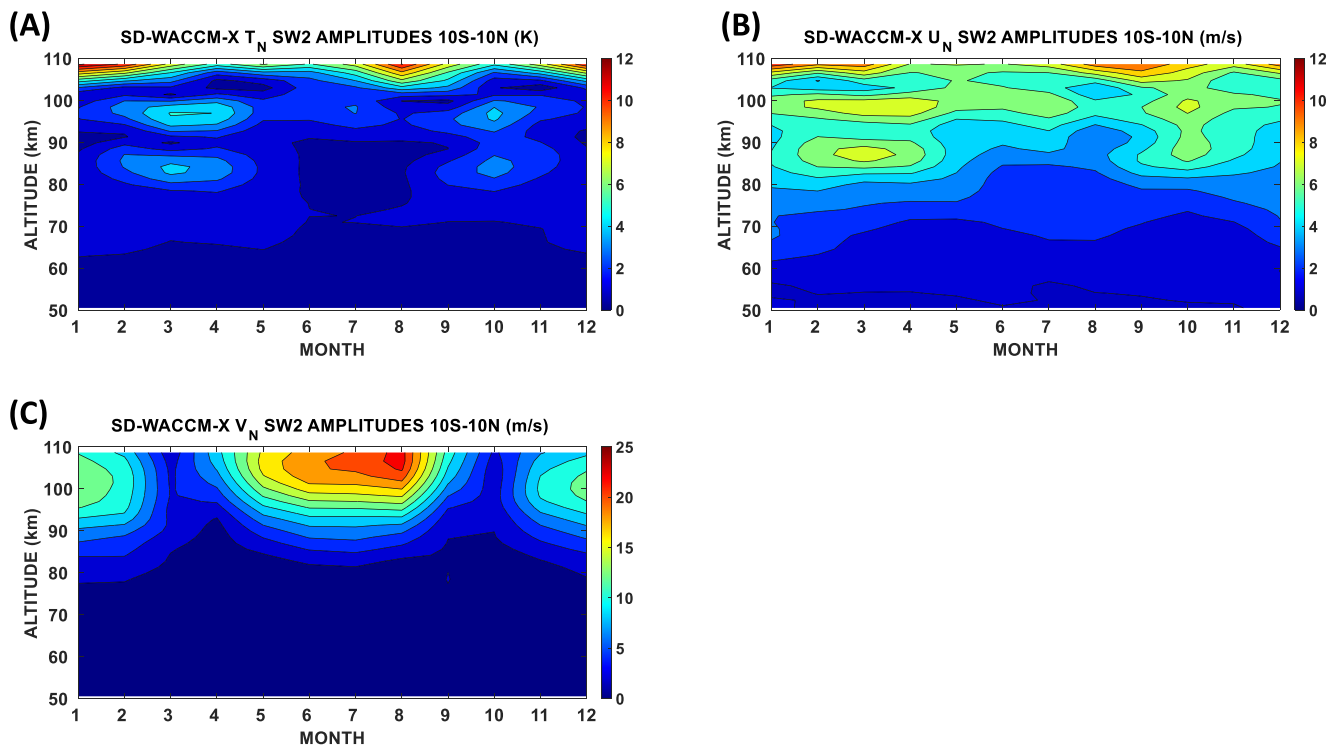


Figure 4. Seasonality of the migrating semidiurnal tide components of tropical upper mesosphere and lower thermosphere temperature (a), zonal wind (b), and meridional wind (c). They are all functions of altitude and month. Units are specified on the plots.

allows MLS to provide near-global maps of 2 a.m. and 2 p.m. temperature from the stratosphere to the upper mesosphere. This work utilizes the longitude and UT information of Aura MLS version 4.2x (V4.2x) temperature observations (https://mls.jpl.nasa.gov/data/v4-2_data_quality_document.pdf).

2.2.2. Alias Test

Following D. L. Wu et al. (1995) and Forbes and Wu (2006), our alias test begins by synthesizing a test cosine signal using specified longitude and UT information. The signal is given by

$$N(\lambda, t) = \hat{N} \cos(n\Omega t_{UT} - s\lambda) \quad (11)$$

Synthesizing this signal gives a set of profiles that are then subject to two-dimensional least squares fit. However, instead of performing the fit across a spectrum of waves simultaneously, the fit is performed across a spectrum of waves individually. Performing a fit individually allows us to calculate amplitudes with aliasing due solely to a given wave. For example, if we synthesize an SW2 tide then do a fit for DW1, the calculated amplitude will only reflect alias values from SW2 (if there is). On the other hand, if we do a fit for DW1 and another nonmigrating tide simultaneously, the calculated amplitudes will be affected by aliasing from the other nonmigrating tide (if SW2 also aliases into the other nonmigrating tide).

3. Results and Discussion

3.1. Seasonal Climatology of SD-WACCM-X Temperature, Zonal-Wind, and Meridional Wind's SW2 Component

To calculate the seasonal climatology of tropical UMLT temperature, zonal-wind, and meridional wind's SW2 component, we first averaged SD-WACCM-X-simulated temperature, zonal wind, and meridional wind between latitudes 10°S and 10°N. Then, from these, we calculate their SW2 amplitudes and phases using 2D least squares fit. Figure 4 shows the seasonal climatology of the SW2 component of temperature, zonal wind, and meridional wind averaged between latitudes 10°S and 10°N. Figures 4a and 4b show that the seasonality of tropical UMLT temperature and zonal wind's SW2 amplitudes both exhibit a seasonality characterized by the appearance of two

local amplitude peaks between 75 and 105 km during equinox seasons. In March equinox, temperature's (zonal wind's) SW2 amplitudes first show a local peak of around 5 K (7 m/s) at ~87 km, then another local peak of around 7 K (7 m/s) at ~97 km before reaching its highest amplitudes with values greater than 12 K (12 m/s) above 105 km. The peaks around ~97 km extend into July but with a weaker value. The amplitudes in October are lower than the March equinox amplitudes by around 1–2 K (1–2 m/s). On the other hand, Figure 4c shows that the meridional wind's SW2 amplitude solely peak during solstice seasons with largest amplitudes of around 20 m/s at ~105 km in August.

As mentioned, numerous studies using ground-based instruments have observed the presence of at least one peak in the amplitudes of the 12-hr oscillation component of zonal and meridional winds in this same region before the amplitude reaches its largest values above 105 km (Deepa et al., 2006; A. Manson et al., 1999; Reddi & Ramkumar, 1997; Vincent et al., 1998). Du et al. (2007) confirmed using CMAM simulations that the SW2 component does contribute to these 12-hr oscillations. However, nobody has presented observations that temperature's SW2 component also has the same features. Our work here indicates that temperature's SW2 component may also have such features.

Past studies have shown that these features can only be reproduced by 3D models (Davis et al., 2013; Du et al., 2007). Tidal models such as the Forbes and Vial (1989) tidal model and the GSWM cannot reproduce this. Hence, it is argued that classical linear tidal theory is not enough to fully explain the presence of one or two local amplitude peaks in the SW2 component of tropical UMLT zonal wind and meridional wind. However, no work has tried to determine the mechanisms behind these peaks. Although the features are not the same as those seen in the 12-hr components of horizontal winds, these results still indicate that SD-WACCM-X can be used to understand the mechanisms behind these peaks. Hence, for the remainder of this paper, we focus on explaining these local amplitude peaks. We first explain the double amplitude peak in March equinox. Then, we explain the single peak in June solstice.

3.2. March Equinox Double Peak

Figure 5 shows the results of our Hough mode reconstruction and tendency analysis to explain the March equinox double peaks in SD-WACCM-X temperature and zonal-wind SW2 amplitudes. We only show the analysis for these two variables because this double-peak structure is only present in them. We first present the results of our Hough mode reconstruction. Figure 5a shows two subplots. The subplot on the left shows the vertical profile of the amplitude of tropical UMLT temperature's SW2 component in March equinox, the amplitudes of the symmetric SW2 Hough modes, and the amplitude of temperature SW2 reconstructed from all Hough modes (hereafter referred to as reconstructed temperature SW2). The subplot on the right shows the vertical profile of the amplitude of tropical UMLT temperature's SW2 component in March equinox, the amplitudes of the asymmetric SW2 Hough modes, and the amplitude of the reconstructed temperature SW2. Figure 5a shows that the reconstructed temperature SW2's profile also shows a double-peak structure, but the amplitudes are around half of the actual double-peak structure. Of all the modes, only the (2,4) mode shows a double-peak structure found at the altitudes of the double-peak structure in tropical UMLT temperature SW2. The (2,2) mode shows a single local peak at around 85 km. The (2,2) and (2,4) modes have the largest amplitudes of all the modes with the (2,2) mode showing comparable amplitudes to the (2,4) mode between 85 and 90 km. This indicates that for the reconstructed temperature SW2, the (2,4) mode is primarily behind the local peak at around 95 km while both (2,2) and (2,4) modes are primarily behind the local peak at around 85 km. However, since the reconstructed profile's amplitudes are only half of the actual profile's amplitudes, these results indicate that these Hough modes cannot fully explain this double-peak structure in tropical UMLT temperature's SW2 amplitude during March equinox.

Figure 5b shows the same as Figure 5a but for the zonal wind. Figure 5b clearly shows that the reconstruction does not reproduce any hint of the double-peak structure. Thus, Figures 5a and 5b clearly show that mode distortion or mode coupling cannot fully explain these local amplitude peak structures. These results indicate that this double-peak structure during March equinox in the SW2 component of tropical temperature and zonal wind is not primarily due to the distortion of SW2 modes by the background atmosphere. This implies that wave-mean flow interaction is not a primary driver of these peaks.

Now we show the results of our tendency analysis with the thermodynamic equation. Figure 5c shows two subplots. The subplot on the left shows the SW2 amplitude of $\frac{dT_h}{dt}$, the SW2 amplitude of the adiabatic term, the

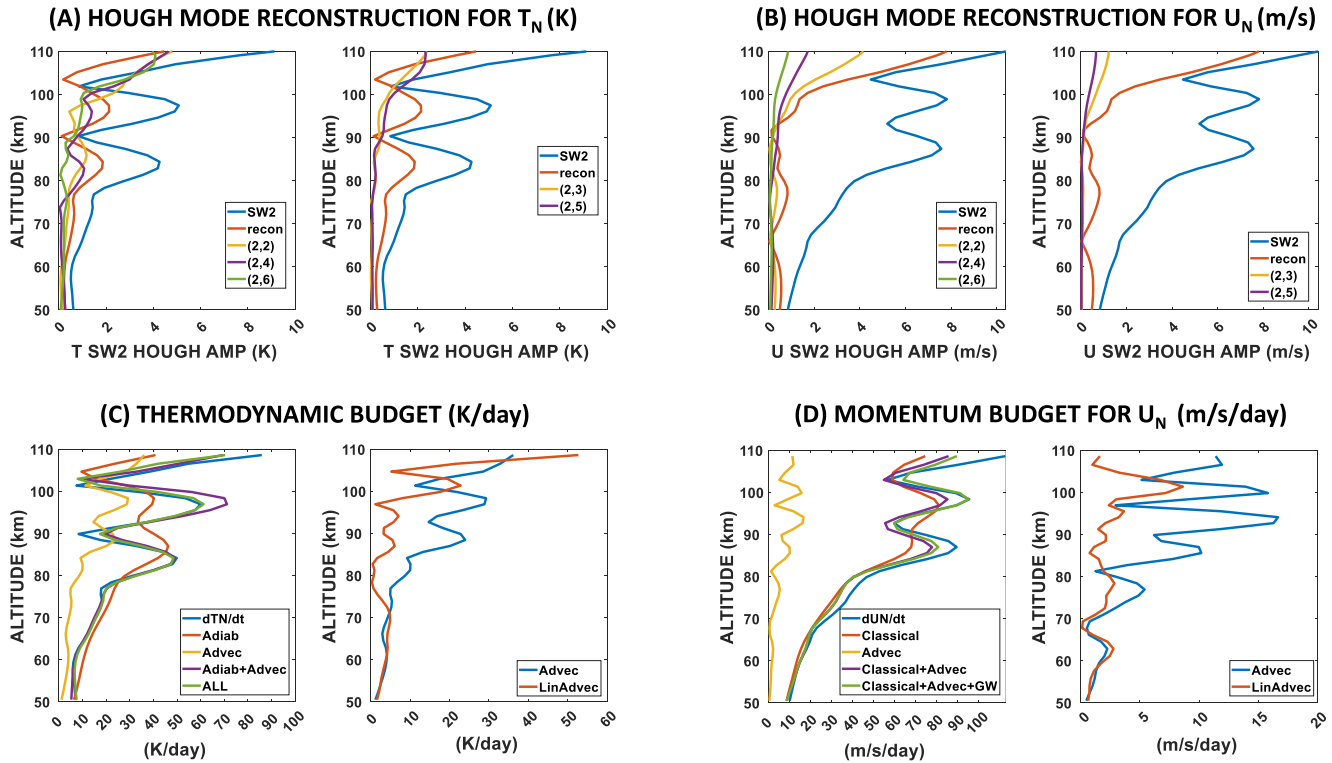


Figure 5. Hough mode reconstruction as well as Hough mode component amplitudes for the migrating semidiurnal tide in tropical upper mesosphere and lower thermosphere (UMLT) temperature (a) and in tropical UMLT zonal wind during March equinox (b). Migrating semidiurnal tide amplitudes of the individual terms in the thermodynamic equation (c) and zonal momentum equation (d) over the tropical UMLT region during March equinox. See text for more details. Units are specified on the plots.

total advection term, the adiabatic term plus the total advection term, and the SW2 amplitude of the sum of all the terms in the thermodynamic equation except $\frac{dT_N}{dt}$. The subplot on the right shows the SW2 amplitudes of temperature total advection and temperature linear advection. This figure shows that the sum of all terms in the thermodynamic equation can satisfactorily reproduce $\frac{dT_N}{dt}$. Looking at the adiabatic terms, we find that the sum of the adiabatic heating due to vertical motion and total advection can reproduce the double-peak structure although the higher peak has a slightly larger amplitude. However, if you look at each term individually, the adiabatic term has a higher amplitude than the total advection term. The adiabatic term shows two peaks, but the features are significantly different from the peaks of $\frac{dT_N}{dt}$. This indicates that the double-peak structure in SW2 temperature requires, at the very least, the sum of both the adiabatic term and total advection term. For the peak at 95 km, it is further shown that diabatic heating terms allow it to match best with the $\frac{dT_N}{dt}$ peak. Figure 5c also shows the contribution of linear advection on the total advection. Linear advection cannot fully explain the total advection. Nonlinear advection is important.

Finally, we show the results of our tendency analysis with the zonal-wind momentum equation. Figure 5d also shows two subplots like Figure 5c. The subplot on the left shows the SW2 amplitude of tropical UMLT $\frac{dU_N}{dt}$, the classical terms (sum of Coriolis force and pressure gradient term), the total advection term, the classical term plus total advection term, and the SW2 amplitudes of the sum of the classical term, total advection term, and gravity wave drag. The subplot on the right shows the SW2 amplitudes of zonal-wind total advection and zonal-wind linear advection. This figure shows that the sum of all terms in the zonal-wind momentum equation can satisfactorily reproduce $\frac{dU_N}{dt}$. Breaking down the terms, this figure shows that the classical terms have the largest contributions, but the features do not satisfactorily match with $\frac{dU_N}{dt}$. This means the winds simply due to the pressure gradient and the Coriolis force will not immediately drive the double-peak structure in zonal wind. The amplitude of total advection is almost an order of magnitude lower than the classical terms. However, this figure shows that you still need advection to at least reproduce a double-peak structure that is close to the double-peak structure of $\frac{dU_N}{dt}$. It is also shown that linear advection cannot fully reproduce the total advection term implying that nonlinear

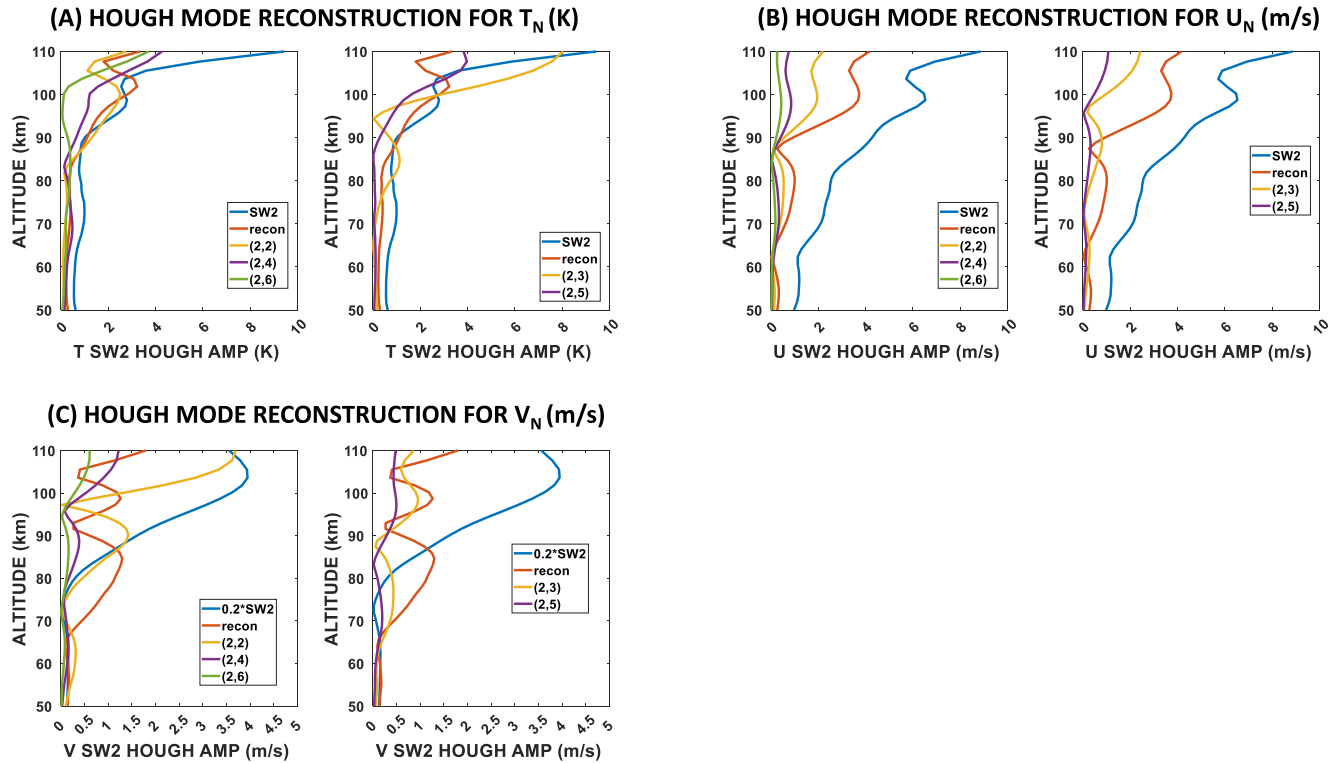


Figure 6. Hough mode reconstruction as well as Hough mode component amplitudes for the migrating semidiurnal tide in tropical upper mesosphere and lower thermosphere (UMLT) temperature (a), in tropical UMLT zonal wind (b), and in tropical UMLT meridional wind (c) during June solstice. See text for more details. Units are specified on the plots.

advection is important. Adding the gravity waves cause the peak at around 95 km to match perfectly with the peak of $\frac{dU_n}{dt}$, while it also improves the peak at around 90 km.

For both the double-peak structure in temperature SW2 and zonal-wind SW2, our results indicate the importance of nonlinear advection. Nonlinear advection involves wave–wave interaction. For the double-peak structure in zonal-wind SW2, apart from wave–wave interaction, our results also indicate the importance of gravity wave drag. The Hough mode reconstruction earlier suggested that wave–mean flow interaction is not a primary driver. Our tendency analysis adds that in situ forcing due to wave–wave interaction and even gravity waves may be important.

3.3. June Solstice Single Peak

Figure 6a shows the same as Figure 5a but for June solstice. Figure 6a shows that the reconstructed temperature SW2's profile reproduces a peak but at a different altitude. The peak in tropical UMLT temperature SW2's amplitude is located between 95 and 100 km, while the peak in the reconstructed temperature SW2's profile is located between 100 and 105 km. Of all the modes, the (2,2) and (2,3) modes have the largest amplitudes between 95 and 105 km. These results indicate that these Hough modes cannot fully explain this single-peak structure in tropical UMLT temperature's SW2 amplitude during June solstice.

Figure 6b shows the same as Figure 5b but for June solstice. Figure 6b shows that the reconstructed zonal-wind SW2's profile only partially reproduces the peak in zonal-wind SW2's amplitude. The reconstructed amplitudes are just lower by 2 m/s. Of all the modes, the (2,2) Hough mode has the largest amplitude followed by the (2,4) Hough mode. These results also indicate that these Hough modes cannot fully explain this single-peak structure in tropical UMLT zonal wind's SW2 amplitude during June solstice.

Figure 6c shows the same as Figure 6b but for meridional wind. Note that the SW2 amplitude of meridional wind is reduced by a factor of 0.2 because the region of peak amplitude above 90 km is 5 times larger than the Hough

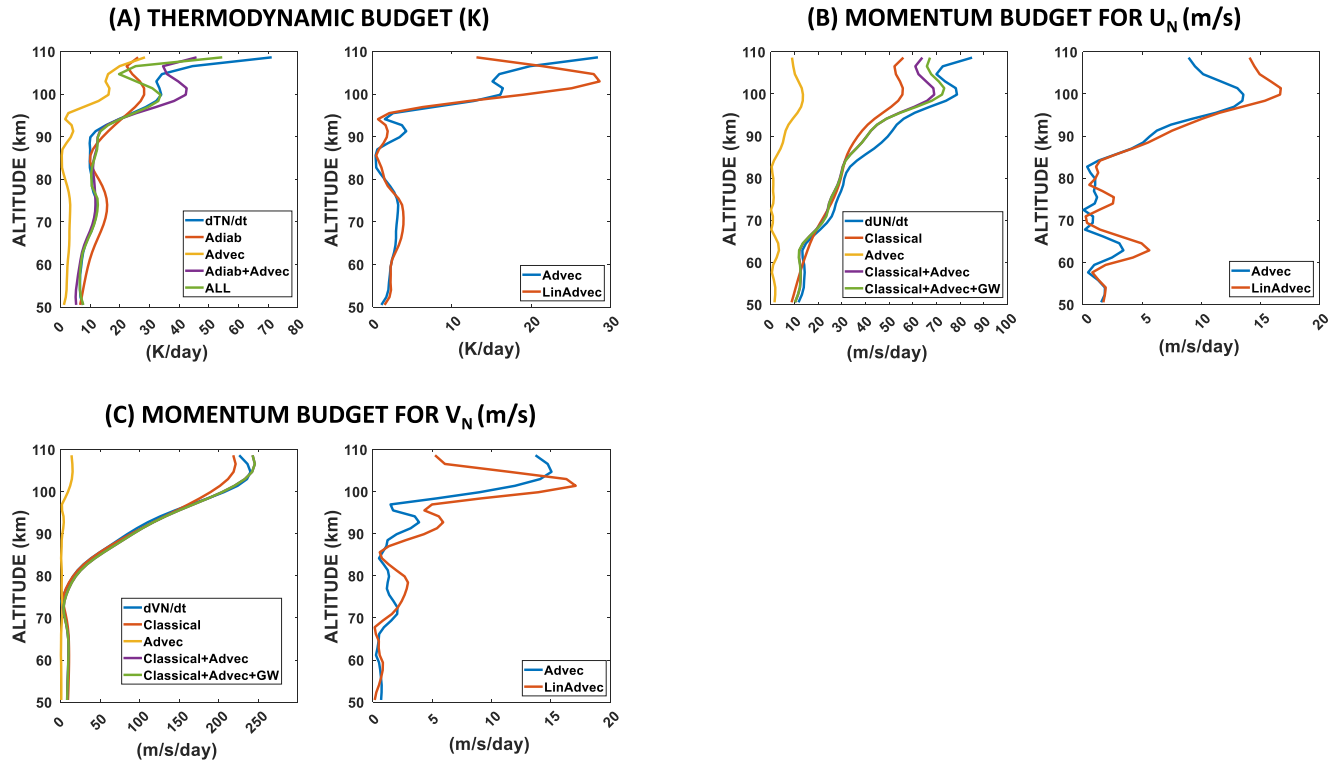


Figure 7. Migrating semidiurnal tide amplitudes of the individual terms in the thermodynamic equation (a), zonal momentum equation (b), and meridional momentum equation (c) over the tropical upper mesosphere and lower thermosphere (UMLT) region during June solstice. See text for more details. Units are specified on the plots.

mode amplitudes. Figure 6c shows that the reconstructed meridional-wind SW2's profile cannot reproduce the peak in meridional-wind SW2's amplitude. Figures 6a–6c clearly indicate that this single-peak structure during June solstice in the SW2 component of tropical temperature, zonal wind, and meridional wind is not primarily due to the distortion of SW2 modes by the background atmosphere. This implies that wave-mean flow interaction is not a primary driver of these peaks. This is the same as the double-peak structure in March equinox temperature SW2 and zonal-wind SW2.

Now we show the results of our tendency analysis with the thermodynamic equation. Figure 7a shows the same as Figure 5c but for June solstice. This figure shows that unlike the double-peak structure in March equinox temperature SW2, the single-peak structure in June solstice temperature SW2 requires all the terms in the thermodynamic equation to satisfactorily reproduce $\frac{dT_N}{dt}$. The sum of the adiabatic term and total advection term can produce the local peak at around 100 km, but the amplitude is larger than the correct amplitude by around 10 K/day. The diabatic term is needed to significantly reduce this difference. Figure 7a also shows the contribution of linear advection on the total advection. Linear advection alone can capture a local peak above 95 km, but it peaks at around 105 km. Also, the amplitude is higher by 10 K/day. This indicates that nonlinear advection is important.

We next show the results of our tendency analysis with the zonal-wind momentum equation. Figure 7b shows the same as Figure 5d but for June solstice. This figure shows that the sum of all terms in the zonal-wind momentum equation can satisfactorily reproduce $\frac{dU_N}{dt}$. Breaking down the terms, this figure shows that the classical terms have the largest contributions, and it does capture the peak at around 100 km although the amplitude is only half the correct amplitude. The amplitude of total advection is almost an order of magnitude lower than the classical terms but combining it with the adiabatic term significantly increases the amplitudes. Figure 7b also shows that linear advection can only partially capture the general structure of the total advection especially the peak at around 100 km. The amplitude of the linear advection term is larger than the total advection term by around 5 m/s/day. Thus, nonlinear advection is also important. When the classical terms and advection are combined, the profile improves with the amplitude only 15 m/s/day lower than the correct amplitude. When gravity waves are added, the difference is further reduced to 10 m/s/day.

Finally, we show the results of our tendency analysis with the meridional-wind momentum equation. Figure 7c shows the same as Figure 7b but for meridional wind. This figure shows that the sum of all terms in the meridional-wind momentum equation can satisfactorily reproduce $\frac{dV_n}{dt}$. Breaking down the terms, Figure 7c shows that the classical terms have the largest contributions, and it does capture the peak at around 100 km with the amplitude already around 85% of the correct amplitude. The amplitude of total advection is 2 orders of magnitude lower than the classical terms but when it is added to the classical terms, the amplitude matches the amplitude of $\frac{dV_n}{dt}$. Linear advection can capture the general structure of the total advection especially the peak at around 100 km, but the amplitude is larger. Thus, nonlinear advection is also important. When gravity waves are added, the difference is negligible. This indicates that the gravity wave drag on the meridional direction is not important.

Like the double-peak structure in March equinox, our results indicate that nonlinear advection and therefore wave–wave interaction is also very important in driving the single-peak structure in temperature SW2, zonal-wind SW2, and meridional-wind SW2 during June solstice. For the single-peak structure in temperature SW2 during June solstice, apart from wave–wave interaction, our results also indicate the importance of diabatic heating terms. For the single-peak structure in zonal-wind SW2 during June solstice, apart from wave–wave interaction, our results also indicate the importance of gravity wave drag. The Hough mode reconstruction earlier suggested that wave-mean flow interaction also is not a primary driver for these single-peak structures. Our tendency analysis adds that in situ forcing due to wave–wave interaction, gravity waves, and diabatic heating may be important.

3.4. Alias Test

The previous sections have shown that wave–wave interaction, gravity waves, and diabatic heating are likely significant contributors to SW2's seasonal variability in the tropical UMLT. Wave–wave interaction and gravity waves are difficult to observe and predict. Since our results suggest that these variabilities may be tied to the presence of SW2 in the tropical UMLT region, we need to be very careful in making assumptions on the presence of SW2 in the tropical UMLT region. Here, we quantify how carelessly ignoring SW2 can affect the calculation of daily-mean zonal mean as well as tides in the tropical UMLT region. This is done through an alias analysis.

Our alias analysis involves synthesizing a signal using the longitude and UT sampling of a particular observational platform. Here, we use SABER and MLS' longitude and UT sampling. In Figure 8a, we synthesized a DW1 signal with 0 daily-mean zonal mean but an amplitude of 10 of arbitrary units using SABER's longitude and UT sampling over the tropics and over 60 days centered on March equinox. From this sampling, we then use 2D least squares fit to scan across all these planetary-scale waves and tides to get their amplitudes. The spectrum is given in this Figure 8a. Here, we can see that for wavenumber -1 and frequency 1 per day which corresponds to DW1, we get the expected amplitude of 10. At the same time, we find that even if the synthesized signal contained no daily-mean zonal mean, a least squares fit finds a daily-mean zonal mean of ~ 2 . There is also an SW2 signal of ~ 7 . These indicate that with SABER's sampling, DW1 can induce a $\sim 20\%$ error in daily-mean zonal-mean values and $\sim 70\%$ error in SW2 amplitudes. In Figure 8b, we synthesized an SW2 signal with 0 daily-mean zonal mean but an amplitude of 10 using SABER's sampling. Figure 8b reveals that this sampling generates a fake DW1 signal with an amplitude of ~ 6 which corresponds to a $\sim 60\%$ error. In Figure 8c, we synthesize the same SW2 signal but using MLS' sampling. Figure 8c reveals that this sampling generates a fictitious daily-mean zonal mean of around 6 which corresponds to a $\sim 60\%$ error.

Most studies that have estimated tides using 2D least squares fit always perform the fit across a spectrum, so these errors are mitigated. But we do have a wide range of other methods now that do not employ 2D least squares fit because their target is the short-term variability of these waves. Our analysis here suggests that over the tropics, these methods must be careful to account for the presence of SW2.

4. Discussions

This work shows that the SD-WACCM-X-simulated seasonality of the SW2 components of tropical UMLT temperature, zonal wind, and meridional wind are characterized by the presence of local peaks in their amplitudes. During equinox seasons, the SW2 components of tropical UMLT temperature and zonal wind have a double-peak structure. During June solstice, the SW2 components of UMLT temperature, zonal wind, and meridional wind have a single-peak structure. Similar features were found in ground-based observations of the 12-hr component of zonal and meridional wind (Deepa et al., 2006; A. Manson et al., 1999; Reddi & Ramkumar, 1997; Vincent

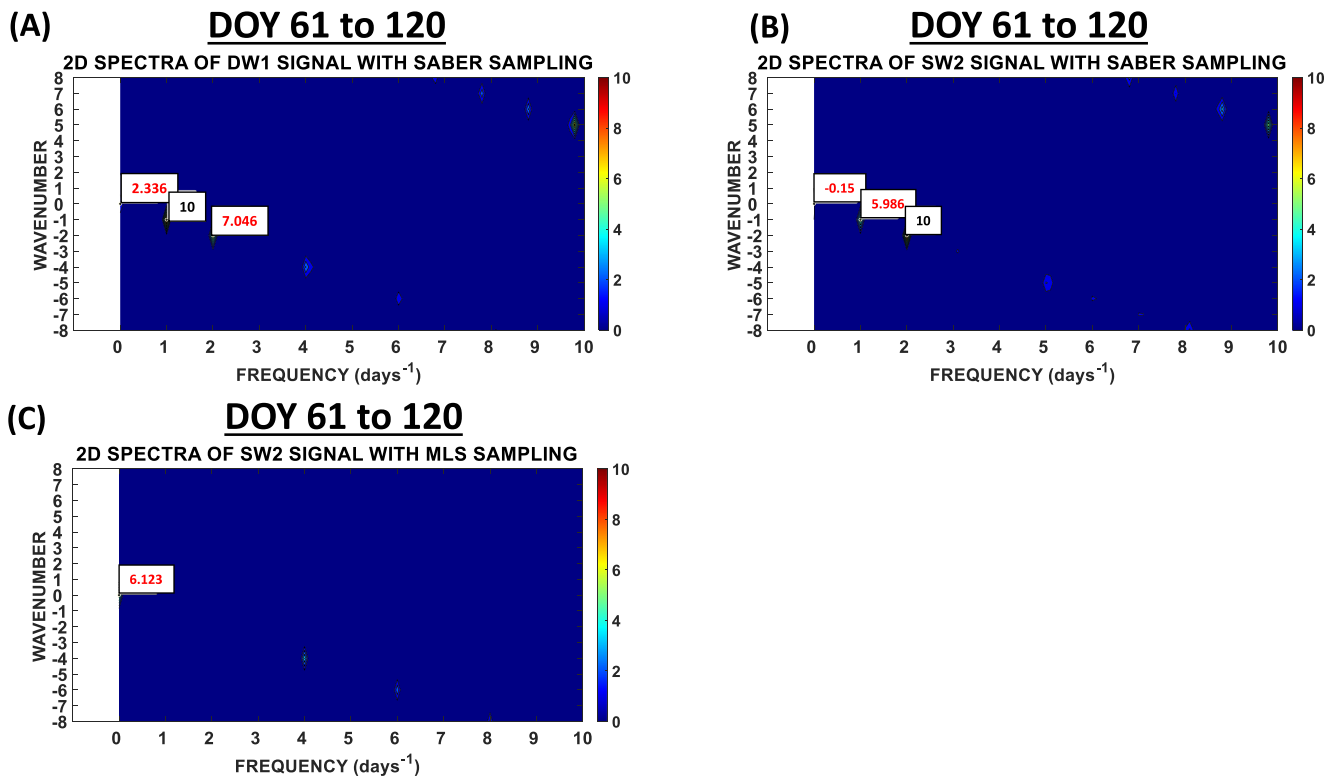


Figure 8. Alias spectra for a DW1 signal (a) and an SW2 signal (b) with amplitude 0 and uses Sounding of the Atmosphere using Broadband Emission Radiometry (SABER) longitude-UT sampling. Alias spectra for an SW2 signal (c) with amplitude 0 and uses Microwave Limb Sounder (MLS) longitude-UT sampling.

et al., 1998). These were also reproduced by other 3D models (Davis et al., 2013; Du et al., 2007). Thus, this work took advantage of SD-WACCM-X's ability to reproduce this to give explanations to the presence of these peaks.

For both the double-peak structure and single-peak structure in tropical UMLT temperature SW2 and zonal-wind SW2, our Hough mode reconstruction suggests that these cannot simply be driven by the background atmosphere's distortion of SW2 Hough modes. Our tendency analysis suggests that in situ generation by wave-wave interaction and gravity waves may be playing major roles. For the single-peak structure in the SW2 component of tropical UMLT temperature, zonal wind, and meridional wind during June solstice, our Hough mode reconstruction also suggests that this cannot simply be driven by the background atmosphere's distortion of SW2 Hough modes. These suggested mechanisms for the seasonality of SW2 in the tropics are very different from the suggested mechanisms for the seasonality of SW2 in the middle to high latitudes. Pedatella et al. (2021) and van Caspel et al. (2022) found that the seasonality of SW2 in the middle to high latitudes can be explained by the background atmosphere's distortion of SW2 modes originating from the stratosphere. However, these do not mean that our results contradict with their results. Tidal variability due to wave-mean flow interaction and due to wave-wave interaction can both occur simultaneously in global scales.

The lower boundary of the Thermosphere Ionosphere Electrodynamics General Circulation model is set at around 97 km and the conditions either come from the GSWM or the CTMT model (Richmond et al., 1992; Roble et al., 1988). The GSWM model does account for gravity wave effects in the form of eddy diffusion, but it does not account for wave-wave interaction nor gravity wave drag (Hagan & Forbes, 2002, 2003). CTMT assumes all tidal variability can be expressed as Hough mode extensions (Oberheide et al., 2011). Thus, CTMT assumes SW2 comes from the lower atmosphere and its variability at ~97 km is primarily driven by wave-mean flow interaction. Our results suggest that these lower boundary conditions are still valid if one is only interested in SW2 variability due to wave-mean flow interaction as well as global-scale phenomena. However, they may not be enough if one would like to also account for SW2 variability due to in situ forcing particularly from wave-wave interaction as well as phenomena solely over the tropics.

Our alias analysis indicates that the zonal-mean component over the tropics as estimated from MLS' sampling may contain alias from SW2 if SW2 has significant amplitude in the region. Taken together with our results showing

that SW2 is closely tied with short-term variability phenomena like wave–wave interaction and gravity waves, our work indicates that one needs to be very careful when calculating the zonal-mean component over the tropics from sun-synchronous satellite observations. One cannot simply assume that SW2's amplitudes are negligible.

5. Summary and Conclusions

This modeling study uses the SD-WACCM-X model to determine and explain the seasonality of SW2 in tropical UMLT temperature, zonal wind, and meridional wind. This work also quantifies how much SW2 affects tidal decomposition using satellite observations. SD-WACCM-X outputs from 2001 to 2019 are used and from these outputs, this work constructs a seasonal climatology of the monthly mean of all parameters (e.g., temperature and winds). Then, these parameters are used to determine and explain the seasonal climatology of tropical UMLT temperature, zonal-wind, and meridional wind's SW2 component.

This work does two model diagnostics. The first diagnostic is a Hough mode reconstruction of SW2 amplitudes in the tropical E-region. This determines if the seasonality of SW2 in the tropical E-region can be explained by the background atmosphere distortion of SW2 modes coming from the lower atmosphere. The second diagnostic is a tendency analysis of the thermodynamic and momentum equations. With the thermodynamic equation, this tendency analysis determines the contributions of linear advection, nonlinear advection, adiabatic heating/cooling, and diabatic heating terms. With the zonal-wind and meridional-wind momentum equations, this tendency analysis determines the contributions of classical terms which include Coriolis force and pressure gradient term as well as the nonclassical terms which include linear advection, nonlinear advection, and gravity wave drag.

Results show that the seasonal climatology of tropical UMLT temperature, zonal-wind, and meridional wind's SW2 component are marked by two features in their amplitudes. One is a double-peak structure in SW2 temperature and zonal-wind amplitude during equinox seasons. The other is a single-peak structure in SW2 temperature, SW2 zonal wind, and SW2 meridional wind in June solstice.

Hough mode reconstruction reveals that for the double-peak structure in March equinox temperature and zonal wind, it cannot be fully reproduced by a linear combination of five SW2 Hough modes. Tendency analysis for the March equinox temperature double-peak structure reveals that it requires, at minimum, both the adiabatic heating/cooling term and the advection term combined. It is further revealed that linear advection alone cannot reproduce the total advection indicating that nonlinear advection is important. Tendency analysis for the March equinox zonal-wind double-peak structure reveals that, at minimum, it requires the classical terms and the advection terms. And, like temperature, linear advection alone cannot reproduce the total advection. If one includes gravity wave drag, the fit is even more improved. Similar mechanisms were found for the June solstice single peak. From these model diagnostics, this work concludes that Hough functions are not a good representation of the seasonality of tropical UMLT SD-WACCM-X temperature SW2, zonal-wind SW2, and meridional-wind SW2 because in situ generation by wave–wave interaction and/or by gravity waves plays a significant role. Their seasonality is not primarily driven by the background atmosphere's distortion of its vertical propagation. Since these mechanisms are related to short-term variability, this work further suggests that SW2's presence in the tropical UMLT is difficult to observe and predict.

Results of our alias analysis indicate that the DW1 component estimated using SABER's sampling in the tropics may have an alias equal to ~60% of SW2's amplitudes. It also indicates that the daily-mean zonal-mean component estimated using MLS' sampling in the tropics may have an alias also equal to ~60% of SW2's amplitudes. From this alias analysis, this work concludes that satellite observations with SABER and MLS' sampling are prone to SW2-related aliasing. This work highly recommends performing similar alias analysis on numerous other observational platforms like the ICON and GOLD missions. Our diagnostics suggest that SW2's presence in the tropical UMLT is difficult to observe and predict, the alias analysis further suggests that one cannot simply assume SW2 in the tropical UMLT is negligible. Future work will determine what specific atmospheric waves could be involved in the wave–wave interactions driving these seasonal features.

Data Availability Statement

As a component of the Community Earth System Model, WACCM-X source code are publicly available at <http://www.cesm.ucar.edu>. The SABER data set presented in this paper is accessible from the SABER website: <http://saber.gats-inc.com/data.php>. The MLS data set presented in this paper is accessible from the MLS website: <https://aura.gsfc.nasa.gov/mls.html>.

Acknowledgments

CCJHS and LCC acknowledge Taiwan National Science and Technology Council (NSTC) Grants 111-2636-M-008-004, 107-2923-M-008-001-MY3, and 110-2923-M-008-005-MY3, as well as the Higher Education SPROUT grant to the Center for Astronautical Physics and Engineering from the Taiwan Ministry of Education. The work of DLW and JNL was supported by NASA's TSIS Project and Sun-Climate research. LQ acknowledges support from the following NASA Grants: 80NSSC19K0278, 80NSSC20K0189, NNH19ZDA001N-HGIO, and NNH19ZDA001N-HSR. HL acknowledges support from NASA Grant 80NSSC20K1323. National Center for Atmospheric Research is a major facility sponsored by the National Science Foundation under Cooperative Agreement No. 1852977. CCJHS is supported by the Taiwan NSTC grants and acknowledges high-performance computing support from Cheyenne (<https://doi.org/10.5065/D6RX99HX>) provided by NCAR's Computational and Information Systems Laboratory, sponsored by the National Science Foundation.

References

- Angelats i Coll, M., & Forbes, J. M. (2002). Nonlinear interactions in the upper atmosphere: The $s = 1$ and $s = 3$ nonmigrating semidiurnal tides. *Journal of Geophysical Research*, 107(A8), 1157. <https://doi.org/10.1029/2001JA900179>
- Burrage, M. D., Hagan, M. E., Skinner, W. R., Wu, D. L., & Hays, P. B. (1995). Long-term variability in the solar diurnal tide observed by HRDI and simulated by the GSWM. *Geophysical Research Letters*, 22(19), 2641–2644. <https://doi.org/10.1029/95GL02635>
- Burrage, M. D., Wu, D. L., Skinner, W. R., Ortland, D. A., & Hays, P. B. (1995). Latitude and seasonal dependence of the semidiurnal tide observed by the high-resolution Doppler imager. *Journal of Geophysical Research*, 100(D6), 11313–11321. <https://doi.org/10.1029/95JD00696>
- Chang, L. C., Palo, S. E., & Liu, H. L. (2011). Short-term variability in the migrating diurnal tide caused by interactions with the quasi 2 day wave. *Journal of Geophysical Research*, 116, D12112. <https://doi.org/10.1029/2010JD014996>
- Chapman, S., & Lindzen, R. S. (1970). *Atmospheric tides* (200 pp.). D. Reidel, Norwell, Mass.
- Davis, R. N., Du, J., Smith, A. K., Ward, W. E., & Mitchell, N. J. (2013). The diurnal and semidiurnal tides over Ascension Island (8°S, 14°W) and their interaction with the stratospheric quasi-biennial oscillation: Studies with meteor radar, eCMAM and WACCM. *Atmospheric Chemistry and Physics*, 13(18), 9543–9564. <https://doi.org/10.5194/acp-13-9543-2013>
- Deepa, V., Ramkumar, G., Antonita, M., Kumar, K. K., & Sasi, M. N. (2006). Vertical propagation characteristics and seasonal variability of tidal wind oscillations in the MLT region over Trivandrum (8.5°N, 77°E): First results from SKIYMET meteor radar. *Annales Geophysicae*, 24(11), 2877–2889. <https://doi.org/10.5194/angeo-24-2877-2006>
- Du, J., Ward, W. E., Oberheide, J., Nakamura, T., & Tsuda, T. (2007). Semidiurnal tides from the extended Canadian Middle Atmosphere Model (CMAM) and comparisons with TIMED Doppler interferometer (TIDI) and meteor radar observations. *Journal of Atmospheric and Solar-Terrestrial Physics*, 69(17–18), 2159–2202. <https://doi.org/10.1016/j.jastp.2007.07.014>
- Forbes, J. M. (1982). Atmospheric tides: 2. The solar and lunar semidiurnal components. *Journal of Geophysical Research*, 87(A7), 5241–5252. <https://doi.org/10.1029/JA087iA07p05241>
- Forbes, J. M., & Garrett, H. B. (1979). Theoretical studies of atmospheric tides. *Reviews of Geophysics*, 17(8), 1951–1981. <https://doi.org/10.1029/RG017i008p01951>
- Forbes, J. M., Makarov, N. A., & Portnyagin, Y. I. (1995). First results from the meteor radar at South Pole: A large 12-hour oscillation with zonal wavenumber one. *Geophysical Research Letters*, 22(23), 3247–3250. <https://doi.org/10.1029/95GL03370>
- Forbes, J. M., & Vial, F. (1989). Monthly simulations of the solar semidiurnal tide in the mesosphere and lower thermosphere. *Journal of Atmospheric and Terrestrial Physics*, 51(7–8), 649–661. [https://doi.org/10.1016/0021-9169\(89\)90063-9](https://doi.org/10.1016/0021-9169(89)90063-9)
- Forbes, J. M., & Wu, D. (2006). Solar tides as revealed by measurements of mesosphere temperature by the MLS experiment on UARS. *Journal of the Atmospheric Sciences*, 63(7), 1776–1797. <https://doi.org/10.1175/jas3724.1>
- Forbes, J. M., & Zhang, X. (2017). The quasi-6 day wave and its interactions with solar tides. *Journal of Geophysical Research: Space Physics*, 122, 4764–4776. <https://doi.org/10.1002/2017JA023954>
- Forbes, J. M., Zhang, X., Palo, S., Russell, J., Mertens, C. J., & Mlynarczyk, M. (2008). Tidal variability in the ionospheric dynamo region. *Journal of Geophysical Research*, 113, A02310. <https://doi.org/10.1029/2007JA012737>
- Gu, H., & Du, J. (2018). On the roles of advection and solar heating in seasonal variation of the migrating diurnal tide in the stratosphere, mesosphere, and lower thermosphere. *Atmosphere*, 9(11), 440. <https://doi.org/10.3390/atmos9110440>
- Hagan, M. E., & Forbes, J. M. (2002). Migrating and nonmigrating diurnal tides in the middle and upper atmosphere excited by tropospheric latent heat release. *Journal of Geophysical Research*, 107(D24), 4754. <https://doi.org/10.1029/2001JD001236>
- Hagan, M. E., & Forbes, J. M. (2003). Migrating and nonmigrating semidiurnal tides in the upper atmosphere excited by tropospheric latent heat release. *Journal of Geophysical Research*, 108(A2), 1062. <https://doi.org/10.1029/2002JA009466>
- Limpasuvan, V., Orsolini, Y. J., Chandran, A., Garcia, R. R., & Smith, A. K. (2016). On the composite response of the MLT to major sudden stratospheric warming events with elevated stratopause. *Journal of Geophysical Research: Atmospheres*, 121, 4518–4537. <https://doi.org/10.1002/2015JD024401>
- Lindzen, R. S., & Hong, S.-S. (1974). Effects of mean winds and meridional temperature gradients on solar and lunar semidiurnal tides in the atmosphere. *Journal of the Atmospheric Sciences*, 31(5), 1421–1466. [https://doi.org/10.1175/1520-0469\(1974\)031<1421:EOMWAH>2.0.CO;2](https://doi.org/10.1175/1520-0469(1974)031<1421:EOMWAH>2.0.CO;2)
- Liu, H. L., Bardeen, C. G., Foster, B. T., Lauritzen, P., Liu, J., Lu, G., et al. (2018). Development and validation of the Whole Atmosphere Community Climate Model with thermosphere and ionosphere extension (WACCM-X 2.0). *Journal of Advances in Modeling Earth Systems*, 10, 381–402. <https://doi.org/10.1002/2017MS001232>
- Liu, J., Liu, H.-L., Wang, W., Burns, A. G., Wu, Q., Gan, Q., et al. (2018). First results from the ionospheric extension of WACCM-X during the deep solar minimum year of 2008. *Journal of Geophysical Research: Space Physics*, 123, 1534–1553. <https://doi.org/10.1002/2017JA025010>
- Lu, X., Liu, H. L., Liu, A. Z., Yue, J., McInerney, J. M., & Li, Z. (2012). Momentum budget of the migrating diurnal tide in the Whole Atmosphere Community Climate Model at vernal equinox. *Journal of Geophysical Research*, 117, D07112. <https://doi.org/10.1029/2011JD017089>
- Manson, A., Meek, C., Hagan, M., Hall, C., Hocking, W., MacDougall, J., et al. (1999). Seasonal variations of the semi-diurnal and diurnal tides in the MLT: Multi-year MF radar observations from 2 to 70 N, and the GSWM tidal model. *Journal of Atmospheric and Solar-Terrestrial Physics*, 61(11), 809–828. [https://doi.org/10.1016/S1364-6826\(99\)00045-0](https://doi.org/10.1016/S1364-6826(99)00045-0)
- Manson, A. H., Luo, Y., & Meek, C. (2002). Global distributions of diurnal and semi-diurnal tides: Observations from HRDI-UARS of the MLT region. *Annales Geophysicae*, 20(11), 1877–1890.
- Marsh, D. R., Mills, M. J., Kinnison, D. E., Lamarque, J. F., Calvo, N., & Polvani, L. M. (2013). Climate change from 1850 to 2005 simulated in CESM1 (WACCM). *Journal of Climate*, 26(19), 7372–7391. <https://doi.org/10.1175/JCLI-D-12-00558.1>
- McLandress, C., Shepherd, G. G., & Solheim, B. H. (1996). Satellite observations of thermospheric tides: Results from the wind imaging interferometer on UARS. *Journal of Geophysical Research*, 101(D2), 4093–4114. <https://doi.org/10.1029/95JD03359>
- Oberheide, J., Forbes, J. M., Zhang, X., & Bruinsma, S. (2011). Climatology of upward propagating diurnal and semidiurnal tides in the thermosphere. *Journal of Geophysical Research*, 116, A11306. <https://doi.org/10.1029/2011JA016784>
- Oberheide, J., Hagan, M. E., & Roble, R. G. (2003). Tidal signatures and aliasing in temperature data from slowly precessing satellites. *Journal of Geophysical Research*, 108(A2), 1055. <https://doi.org/10.1029/2002JA009585>
- Oberheide, J., Wu, Q., Killeen, T. L., Hagan, M. E., & Roble, R. G. (2007). A climatology of nonmigrating semidiurnal tides from TIMED Doppler Interferometer (TIDI) wind data. *Journal of Atmospheric and Solar-Terrestrial Physics*, 69(17–18), 2203–2218. <https://doi.org/10.1016/j.jastp.2007.05.010>
- Palo, S. E., Roble, R. G., & Hagan, M. E. (1999). Middle atmosphere effects of the quasi two-day wave determined from a General Circulation Model. *Earth, Planets and Space*, 51(7–8), 629–647. <https://doi.org/10.1186/bf03353221>
- Pancheva, D., Mukhtarov, P., & Andonov, B. (2009). Global structure, seasonal and interannual variability of the migrating semidiurnal tide seen in the SABER/TIMED temperatures (2002–2007). *Annales Geophysicae*, 27(2), 687–703. <https://doi.org/10.5194/angeo-27-687-2009>

- Pedatella, N. M., & Forbes, J. M. (2010). Evidence for stratosphere sudden warming-ionosphere coupling due to vertically propagating tides. *Geophysical Research Letters*, 37, L11104. <https://doi.org/10.1029/2010GL043560>
- Pedatella, N. M., Liu, H. L., Conte, J. F., Chau, J. L., Hall, C., Jacobi, C., et al. (2021). Migrating semidiurnal tide during the September equinox transition in the Northern Hemisphere. *Journal of Geophysical Research: Atmospheres*, 126, e2020JD033822. <https://doi.org/10.1029/2020JD033822>
- Reddi, C. R., & Ramkumar, G. (1997). Climatologies of tidal winds in the radio-meteor region over Trivandrum (8 N). *Journal of Atmospheric and Solar-Terrestrial Physics*, 59(14), 1757–1777. [https://doi.org/10.1016/s1364-6826\(97\)00042-4](https://doi.org/10.1016/s1364-6826(97)00042-4)
- Richmond, A. D., Ridley, E. C., & Roble, R. G. (1992). A thermosphere/ionosphere general circulation model with coupled electrodynamics. *Geophysical Research Letters*, 19(6), 601–604. <https://doi.org/10.1029/92GL00401>
- Rienecker, M. M., Suarez, M. J., Gelaro, R., Todling, R., Bacmeister, J., Liu, E., et al. (2011). MERRA: NASA's Modern-Era Retrospective Analysis for Research and Applications. *Journal of Climate*, 24(14), 3624–3648. <https://doi.org/10.1175/JCLI-D-11-00015.1>
- Roble, R. G., Ridley, E. C., Richmond, A. D., & Dickinson, R. E. (1988). A coupled thermosphere/ionosphere general circulation model. *Geophysical Research Letters*, 15(12), 1325–1328. <https://doi.org/10.1029/GL015i012p01325>
- Russell, J. M., III, Mlynczak, L. L., Gordley, J. J., Tansock, L. L., & Esplin, R. W. (1999). Overview of the SABER experiment and preliminary calibration results. *Proceedings of SPIE*, 3756, 277–288. <https://doi.org/10.1117/12.366382>
- Teitelbaum, H., & Vial, F. (1991). On tidal variability induced by nonlinear interaction with planetary waves. *Journal of Geophysical Research*, 96(14), 14169–14178. <https://doi.org/10.1029/91JA01019>
- Teitelbaum, H., Vial, F., Manson, A. H., Giraldez, R., & Massbeuf, M. (1989). Non-linear interaction between the diurnal and semidiurnal tides: Terdiurnal and diurnal secondary waves. *Journal of Atmospheric and Terrestrial Physics*, 51(7–8), 627–634. [https://doi.org/10.1016/0021-9169\(89\)90061-5](https://doi.org/10.1016/0021-9169(89)90061-5)
- van Caspel, W. E., Espy, P. J., Ortland, D. A., & Hibbins, R. E. (2022). The mid- to high-latitude migrating semidiurnal tide: Results from a mechanistic tide model and SuperDARN observations. *Journal of Geophysical Research: Atmospheres*, 127, e2021JD036007. <https://doi.org/10.1029/2021JD036007>
- Vincent, R. A., Kovalam, S., Fritts, D. C., & Isler, J. R. (1998). Long-term MF radar observations of solar tides in the low-latitude mesosphere: Interannual variability and comparisons with the GSWM. *Journal of Geophysical Research*, 103(D8), 8667–8683. <https://doi.org/10.1029/98JD00482>
- Walterscheid, R. L., & Venkateswaran, S. V. (1979a). Influence of mean zonal motion and meridional temperature gradients on the solar semidiurnal atmospheric tide: A spectral study. Part 1: Theory. *Journal of the Atmospheric Sciences*, 36(9), 1623–1635. [https://doi.org/10.1175/1520-0469\(1979\)036<1623:IOMZMA>2.0.CO;2](https://doi.org/10.1175/1520-0469(1979)036<1623:IOMZMA>2.0.CO;2)
- Walterscheid, R. L., & Venkateswaran, S. V. (1979b). Influence of mean zonal motion and meridional temperature gradients on the solar semidiurnal atmospheric tide: A spectral study. Part 2: Numerical results. *Journal of the Atmospheric Sciences*, 36(9), 1636–1662. [https://doi.org/10.1175/1520-0469\(1979\)036<1636:IOMZMA>2.0.CO;2](https://doi.org/10.1175/1520-0469(1979)036<1636:IOMZMA>2.0.CO;2)
- Wu, D. L., Hays, P. B., & Skinner, W. R. (1995). A least squares method for spectral analysis of space-time series. *Journal of the Atmospheric Sciences*, 52(20), 3501–3511. [https://doi.org/10.1175/1520-0469\(1995\)052<3501:ALSMFS>2.0.CO;2](https://doi.org/10.1175/1520-0469(1995)052<3501:ALSMFS>2.0.CO;2)
- Wu, Q., Killeen, T. L., Nozawa, S., McEwen, D., Guo, W., & Solomon, S. C. (2003). Observations of mesospheric neutral wind 12-hour wave in the Northern Polar Cap. *Journal of Atmospheric and Solar-Terrestrial Physics*, 65(8), 971–978. [https://doi.org/10.1016/s1364-6826\(03\)00116-0](https://doi.org/10.1016/s1364-6826(03)00116-0)
- Wu, Q., Killeen, T. L., Ortland, D. A., Solomon, S. C., Gablehouse, R. D., Johnson, R. M., et al. (2006). TIMED Doppler interferometer (TIDI) observations of migrating diurnal and semidiurnal tides. *Journal of Atmospheric and Solar-Terrestrial Physics*, 68(3–5), 408–417. <https://doi.org/10.1016/j.jastp.2005.02.031>
- Wu, Q., Ortland, D., Solomon, S., Skinner, W., & Niciejewski, R. (2011). Global distribution, seasonal, and inter-annual variations of mesospheric semidiurnal tide observed by TIMED TIDI. *Journal of Atmospheric and Solar-Terrestrial Physics*, 73(17), 2482–2502. <https://doi.org/10.1016/j.jastp.2011.08.007>
- Yamashita, K., Miyahara, S., Miyoshi, Y., Kawano, K., & Ninomiya, J. (2002). Seasonal variation of non-migrating semidiurnal tide in the polar MLT region in a general circulation model. *Journal of Atmospheric and Solar-Terrestrial Physics*, 64(8–11), 1083–1094. [https://doi.org/10.1016/s1364-6826\(02\)00059-7](https://doi.org/10.1016/s1364-6826(02)00059-7)
- Yuan, T., Schmidt, H., She, C. Y., Krueger, D. A., & Reising, S. (2008). Seasonal variations of semidiurnal tidal perturbations in mesopause region temperature and zonal and meridional winds above Fort Collins, Colorado (40.6 N, 105.1 W). *Journal of Geophysical Research*, 113, D20103. <https://doi.org/10.1029/2007JD009687>
- Zhang, J., Limpasuvan, V., Orsolini, Y. J., Espy, P. J., & Hibbins, R. E. (2021). Climatological westward-propagating semidiurnal tides and their composite response to sudden stratospheric warmings in SuperDARN and SD-WACCM-X. *Journal of Geophysical Research: Atmospheres*, 126, e2020JD032895. <https://doi.org/10.1029/2020JD032895>
- Zhang, X., Forbes, J. M., Hagan, M. E., Russell, J. M., III, Palo, S. E., Mertens, C. J., & Mlynczak, M. G. (2006). Monthly tidal temperatures 20–120 km from TIMED/SABER. *Journal of Geophysical Research*, 111, A10S08. <https://doi.org/10.1029/2005JA011504>